



A Specifically Designed Injector for Controlled Lube Oil Addition in View of Investigation of Pre-Ignition Phenomena in Dual-Fuel/Gas Engines

Pascal Süess*, Bruno Schneider, Dario Wüthrich, Silas Wüthrich and Kai Herrmann

Institute of Thermal and Fluid Engineering (ITFE), School of Engineering (HST), University of Applied Sciences and Arts Northwestern Switzerland (FHNW), Windisch, Switzerland

OPEN ACCESS

Edited by:

Panayotis Dimopoulos Eggenschwiler,
Swiss Federal Laboratories for
Materials Science and Technology,
Switzerland

Reviewed by:

Hui Zhang,
Beihang University, China
Alpaslan Atmanli,
National Defense University, Turkey

*Correspondence:

Pascal Süess
pascal.suess@fnw.ch

Specialty section:

This article was submitted to
Engine and Automotive Engineering,
a section of the journal
Frontiers in Mechanical Engineering

Received: 30 October 2020

Accepted: 03 February 2021

Published: 11 May 2021

Citation:

Süess P, Schneider B, Wüthrich D,
Wüthrich S and Herrmann K (2021) A
Specifically Designed Injector for
Controlled Lube Oil Addition in View of
Investigation of Pre-Ignition
Phenomena in Dual-Fuel/Gas Engines.
Front. Mech. Eng 7:623896.
doi: 10.3389/fmech.2021.623896

Internal combustion engines will continue to play a role during a transitional phase, especially in heavy-duty or marine applications. In this context, lean-burn gas/dual-fuel combustion is an attractive concept to reduce CO₂, combined with considerably lower particulate and NO_x pollution, and with efficiencies comparable to diesel combustion. However, ignition processes still pose considerable challenges, with pre-ignition in particular being a major issue. The underlying mechanisms are probably based on self-ignition of lube oil in hot zones. In order to investigate fundamentals of such phenomena in optically accessible test rigs, a novel injector was specifically developed to induce pre-ignitions artificially. The so-called “PieZo-Droplet-Injector” (PZDI) enables dosing of minor amounts of lubricating oil or even the injection of single droplets with diameters in the range of 100–200 μm. The working principle relies on a needle actuated with a piezo stack, which pushes a certain amount of lube oil in a bore so that (even single) droplets can be ejected through an adjustable nozzle. To confirm the PZDI functionality and to investigate droplet characteristics based on adjustable operating parameters, tests were performed under ambient conditions as well as in a constant volume combustion chamber under reasonable pressure and temperature conditions. Overall, the PZDI showed an excellent behavior in terms of capabilities to inject small amounts or even single droplets of lube oil. At last, this specially developed injector allows selective lube oil addition in an optically accessible engine test facility for upcoming examination of pre-ignition phenomena under real operating conditions.

Keywords: lube oil, lubricating oil, pre-ignition, gas engine, dual-fuel engine, injector, droplet, IC engine

INTRODUCTION

Internal combustion engines of today have progressed to efficient and reliable machines. Even though the electrification of individual transport increases, they will probably remain the dominant propulsion source for heavy-duty or marine freight transportation. In view of emission legislation, combustion processes need to be improved and carbon-reduced or alternative (renewable) fuels considered. In the marine sector, so-called dual-fuel engines feature efficiency comparable to a diesel engine with reduced CO₂ and considerably lower particulate as well as NO_x emissions. In the underlying (low temperature) combustion concept, ignition of a lean premixed gas/air charge by a pilot fuel or reactive jet takes place. However, with increasing efficiencies, a reliable operating range

becomes more and more limited due to “knocking” or “misfiring” effects. Moreover, unwanted pre-ignition can appear since the premixed charge under high pressure and temperature conditions is susceptible to early ignition phenomena. The phenomenon of pre-ignition occurring in Otto-principle (gasoline, gas, dual-fuel) engines, where the premixed combustible charge can ignite before the actual ignition by a spark plug, pilot injection or reactive jet, causes steep pressure gradients and high peak pressures, respectively temperatures that can even damage the engine. Typical origins for pre-ignition can be hot surfaces in the combustion chamber or soot deposits on walls or valves. In any case, examination on its causes and possible countermeasures are still object of current research investigations.

An overview of pre-ignition sources and their classification with respect to automotive application is given in (Dahnz et al., 2009; Palaveev, 2013). As origin respectively main influences, lube oil spray-wall interaction (oil type/additives), locally hot cylinder and cover wall temperatures (“hot spots”) and subsequent pre-ignitions caused by early ignition events of previous cycles were identified. Increased boost levels of downsized gasoline engines led to an identical behavior, especially at low speed and wide open throttle (WOT) conditions (Mayer et al., 2016). In addition, the examination of various lubricating oil detergents revealed that calcium in particular could promote pre-ignition. In (Welling et al., 2014; Long et al., 2016), a standard injector was used to insert oil into the combustion chamber of a non-optical test engine in order to artificially induce pre-ignitions.

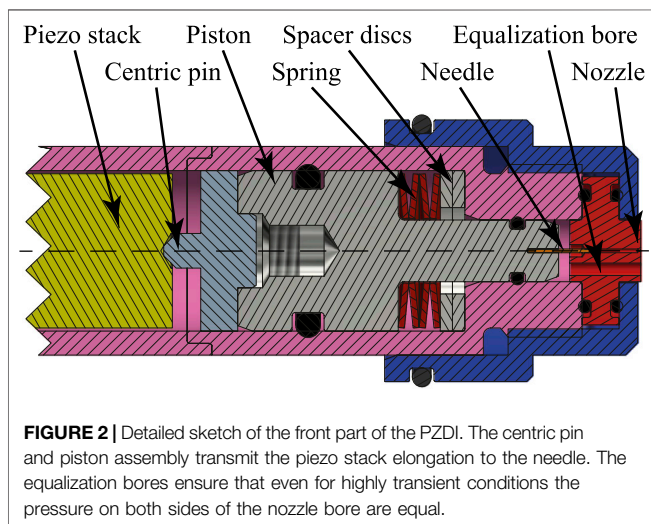
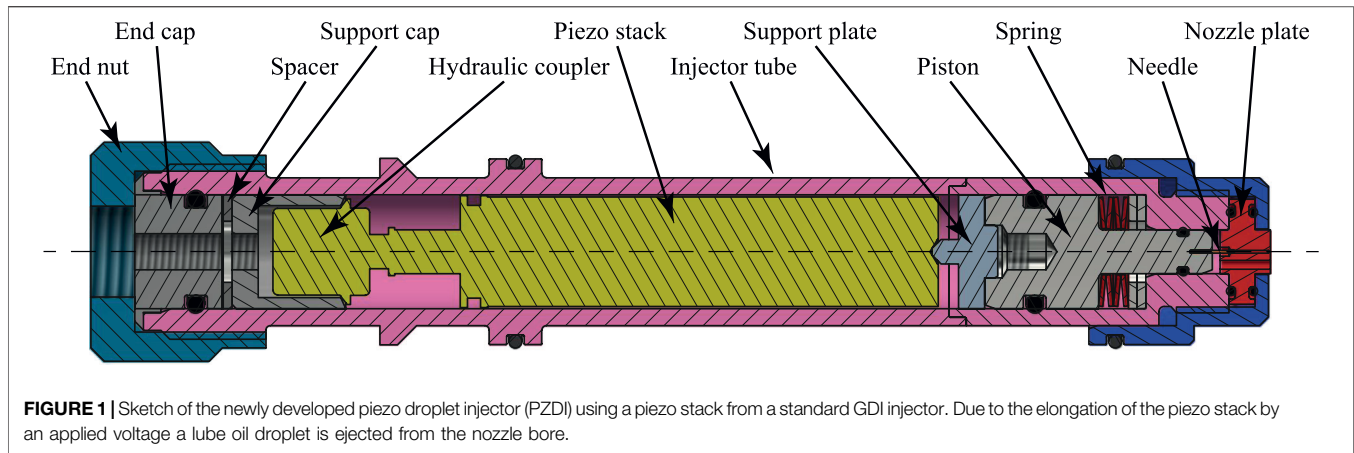
On the marine application side, general possible origin and influencing factors in terms of pre-ignition were identified by (Imhof and Takasaki, 2012; Imhof, 2013), such as lube oil in the combustion chamber, high compression temperature, and in-cylinder charge composition. For large dual-fuel engines, characteristic pre-ignition phenomena could be observed, where pre-ignition occurs sporadically within a limited range of advanced timing crank angles and with less increase of peak firing pressure (Yasueda et al., 2012). In gas engines with high break mean effective pressures (BMEP), the compression temperature exceeds the auto-ignition temperature of the lubricating oil, which differs not much from the fuel oil. It may lead to evaporation and ignition of residual oil and possible further inflammation of the premixed air-gas-charge. This is the reason for the above-mentioned limitation of advanced pre-ignition timing, because the charge reaches the oil self-ignition temperature at the end of compression stroke. This phenomenon was optically investigated in a rapid compression expansion machine (RCEM) (Yasueda et al., 2013). In large two-stroke marine engines, lube oil is injected directly into the piston ring pack by so-called “quills” located in the cylinder liner (Christensen, 2010). Due to this specific liner/piston lubrication concept, droplets or oil ligaments can be present inside the engine combustion chamber being a possible originator for lube oil pre-ignition. The issue of pre-ignition affecting the operation stability (e.g. in-cylinder pressure raise, knocking effects, cycle-to-cycle variation) is even more distinct in large low-speed two-stroke marine gas/dual-fuel engines due to the relatively long period of

high pressure/temperature conditions before ignition and combustion onset takes place.

Fundamental investigation of pre-ignition based on standard quantities obtained from conventional engine test benches is difficult since necessary information on (turbulent) flow field, evaporation and mixing processes, phase transitions and subsequent reactions (uncontrolled inflammation) can usually not be determined. Thus, application at the in-house available optically accessible engine test facility “Flex-OeCoS” (Schneider et al., 2020) with a possibility of selective lube oil addition (and/or presence of “hot spots”) would allow an in-depth examination of the underlying mechanism of the phenomena. Since common fuel injectors are not suitable for this application, because of their hydraulic working principle using high injection pressures, a special injector for controlled lube oil addition had to be developed — the PZDI presented here. Ideally, it should be able to inject quantitatively characterized, small amounts of lube oil or even single droplets into the combustion chamber. Further, it must be able to withstand engine relevant conditions in terms of elevated pressures and temperatures. The intention is to use this newly developed PZDI for more investigations of dual-fuel ignition and combustion processes (Humair et al., 2020), particularly in terms of pre-ignition phenomena. The final aim of the experimental investigations is to gain detailed insight into the processes involved in pre-ignition phenomena, and to generate reference data for the development of corresponding simulation models.

PIEZO DROPLET INJECTOR

Based on a concept found in literature (Ohtomo et al., 2014) a special droplet injector design was developed and realized (PZDI, **Figure 1**). As the key element of the PZDI, the piezo stack from a standard GDI injector is used as actuator. The stack is surrounded by the injector tube, which is made of two parts joined by laser welding. The diameter of the bore was chosen to be slightly larger than the stack. The stack displaces the piston over the support plate having a centric pin similar to the original GDI injector design to avoid bending stresses. The piston has an attached needle ($\varnothing_{\text{needle}} = 290 \mu\text{m}$), which fits into the central bore ($\varnothing_{\text{bore}} = 300 \mu\text{m}$) in the nozzle plate. A screwed cap holds the nozzle plate in place. A more detailed description of the injection mechanism using an enlarged drawing will follow later (see **Figure 2**). The resetting force to move the piston back to its initial position after an injection is provided by disk springs. The preload of these springs can be controlled with spacers, with which the position of the support cap on the other side of the stack can be adjusted. This support cap fixes the hydraulic coupler as in the original injector and compensates different length changes due to thermal expansion. To avoid torsional moment on the piezo stack during tightening of the end nut, the end cap is torsion-proof designed. The bores with the thread in the support cap and end cap are needed for the control cable, and to be able to disassemble the injector. This is also the reason behind the divided design of the piston and the support plate. The thread in the end nut is used for mounting a screwed cable gland to seal the back end of the



injector. The clamp support on the outside of the injector tube is necessary to mount the injector in the test rig.

A detailed view of the injector tip is shown in **Figure 2**. While assembling the PZDI, the bore in the nozzle plate (made of bronze) is filled with lube oil. For an easier filling process and exchange of the nozzle geometry, the nozzle plate was manufactured as a separate component and fixed with a screwed cap. The needle with a slightly smaller diameter as the bore is glued into the piston with retaining compound. The other end slides in the nozzle bore to push the oil volume out through the nozzle hole ($\varnothing_{\text{nozzle}} = 100 \mu\text{m}$). The initial position of the piston (and therefore the needle as well) can be adjusted with spacers between the disc springs and the injector tube front end. The position of the laser welded connection is chosen to be located behind the piston to ensure its proper gliding together with the corresponding O-ring. Pressure equalization bores in the nozzle plate ensure that the pressure behind the nozzle always corresponds to the pressure in front of the injector even for highly transient conditions. Without this pressure equalization, pressure gradients would push the oil out of the lube oil reservoir due to lack of a needle seal. Other seals in the piston and nozzle plate however prevent the pressure from spreading any further into the injector.

EXPERIMENTAL SETUP AND METHODOLOGY

Environmental Conditions

For a first investigation under environmental conditions (room temperature, atmospheric pressure) a measurement setup consisting of a high-speed camera, a diffuse LED light source and a temperature control unit was built (**Figure 3**). The image acquisition technology used was shadow imaging, i.e. the droplet appears as dark shadow in front of a bright background. For the diffuse background illumination, an LED light source with 500 diodes and a diffuser panel was used. A high-speed camera (Photron Fastcam APX-RS) with a Navitar zoom-lens was installed on the opposite side of the injector. To achieve reproducible conditions for droplet generation, the injector was mounted with the adapter for the CVCC to enable controlled heating of the injector with an external temperature control unit. The resulting temperature at the injector tip was measured with a type K thermocouple.

A post-processing procedure evaluated size and position of the droplets from the images. The “Circle Hough Transform” (CHT) method (Atherton and Kerbyson, 1999) was found to be an ideal algorithm to find the droplets. Normally used for circle detection, the CHT can be adapted to find droplets in the captures made with the “shadow imaging” technique because the oil droplets appear like dark circles in front of the bright background. With its robustness even in the presence of noise, occlusions and varying illumination, the method is ideal for this investigation. It works by searching pixels with high brightness gradients, which are used as center of circles. Then, the radii of the new circles are estimated in a separate step. This process is repeated until coincidence in the center of the detected circle occurs. Thus, the center and the radius of the droplet can be determined.

Constant Volume Combustion Chamber

A schematic sketch of the setup at the CVCC is shown in **Figure 4**. The high-speed camera was a Photron SA-X2 with a sample rate up to 400 kHz and a Navitar 12x zoom-lens. Since there is no optical access on the opposite site of the camera, shadow imaging was not possible. Therefore, proper illumination

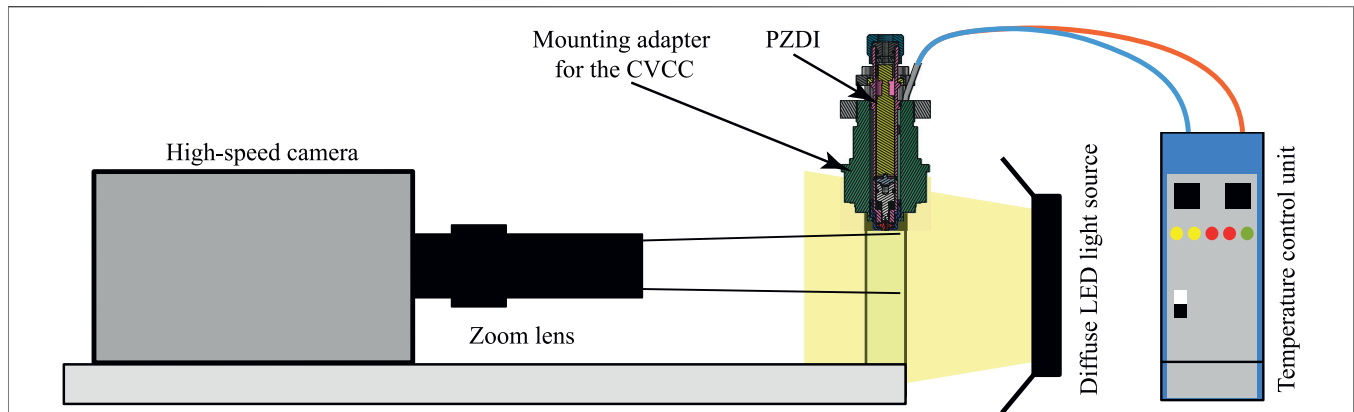


FIGURE 3 | Shadow imaging setup of the PZDI at environmental conditions. The injector is mounted in the adapter normally used for the measurements in the CVCC to condition it to 80°C as in the other experiments.

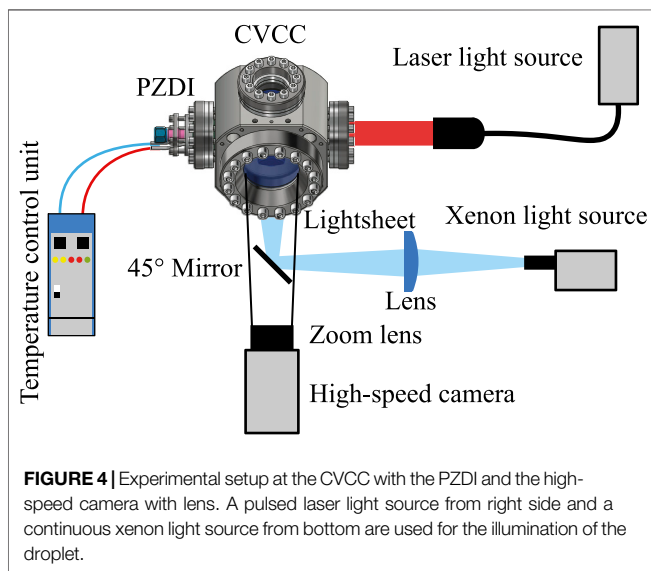


FIGURE 4 | Experimental setup at the CVCC with the PZDI and the high-speed camera with lens. A pulsed laser light source from right side and a continuous xenon light source from bottom are used for the illumination of the droplet.

of the oil droplets was realized with a Cavilux laser unit, which emits monochromatic (687 nm), low-coherence light pulses. The light is transmitted via a fiber optic cable from the laser diode to the front lens which is installed on the opposite side of the injector (right side of the CVCC). In addition, a xenon light source illuminated the droplet through the bottom window of the cell. This light is directed through a rectangular cylinder lens to create a light sheet. The xenon light source is continuous, but the Cavilux laser diode pulses have been synchronized with the high-speed camera. Compared to shadow imaging, the recorded light intensity is much lower, therefore the image acquiring frequency was varied between 5 and 30 kHz to maximize exposure time. To have a constant lube oil temperature independent of the cell temperature, the PZDI was kept at 80°C by the temperature control unit. Normally, the cell can be heated up to 900 K to achieve self-ignition conditions of fuel sprays. For this investigation however, no ignition of the oil was desired. Therefore, the cell was filled with nitrogen (20, 30, 50,

60 bar) and the temperature was adjusted to have a gas temperature of 100°C.

For post-processing the images taken in the CVCC however, another approach had to be chosen because a background illumination, as it is necessary for shadow imaging, is not possible. Thus, the droplet detection was more difficult. As an alternative, the foreground detector (Kaewtrakulpong and Bowden, 2002) implemented in the MATLAB image vision toolbox was adapted for this case. This algorithm is normally used for detecting and tracking moving objects (e.g., persons, cars) on video-based surveillance systems. The algorithm needs to be trained with a chosen number of pictures of the individual background, and additional parameters must be adjusted to avoid detection of smaller objects like moving leaves of trees. For the images taken in the CVCC this feature was used to subtract the stationary background from the moving oil droplets. After training, the routine was able to create binary pictures of the illuminated droplets. With the detection of accumulated pixels in the foreground (e.g., single illuminated droplets) it was possible to track the droplet position through the full set of high-speed captures.

RESULTS AND DISCUSSION

The post-processed results of the experiments at environmental conditions and at elevated pressures in the CVCC are described in the following chapters. An overview of the experimental parameters for the measurements is shown in **Table 1**.

Environmental Conditions

The PZDI was first characterized under environmental conditions. This included a parameter study of driving voltage and energizing time (ET) and their influence on the needle lift as well as droplet formation.

Measurement of Needle Lift

The first step in the characterization of the PZDI was the optical measurement of the needle lift. The measurement setup was similar as shown in **Figure 3**, but without nozzle plate and

TABLE 1 | Overview of the experimental investigation with the PZDI, the varied parameters and the post-processed results.

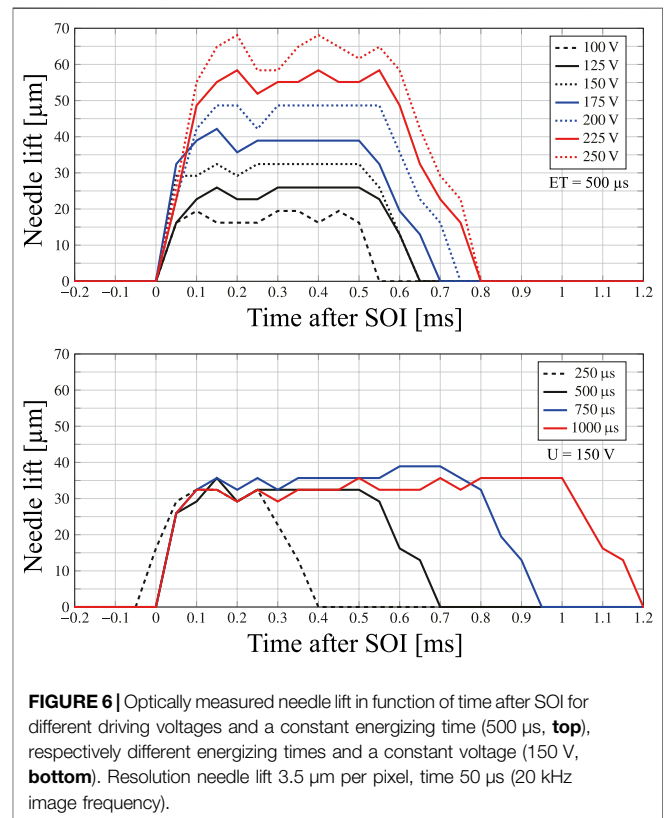
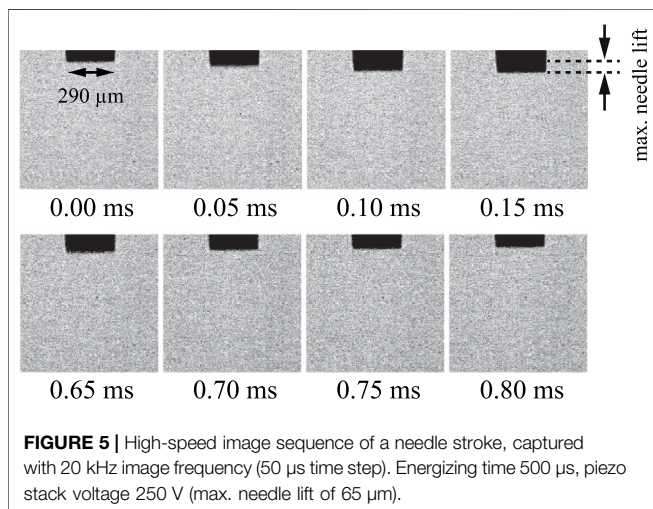
Setup	Optical measurement	Variations	Voltage [V]	ET [μ s]	Injector temperature [°C]	Gas temperature [°C]	Pressure [bar]	Results
Environmental conditions	Needle lift	ET, voltage	100, 125, ..., 250	250, 500, ..., 1000	80	21	Ambient	Needle lift
	Droplet generation	ET, voltage	80, 90, ..., 200	50, 100, ..., 650	80	21	Ambient	Diameter, location, velocity
CVCC	Droplet generation	ET, voltage, pressure	150, 200, 250	500	80	100	20, 30, 50, 60	Location, penetration length

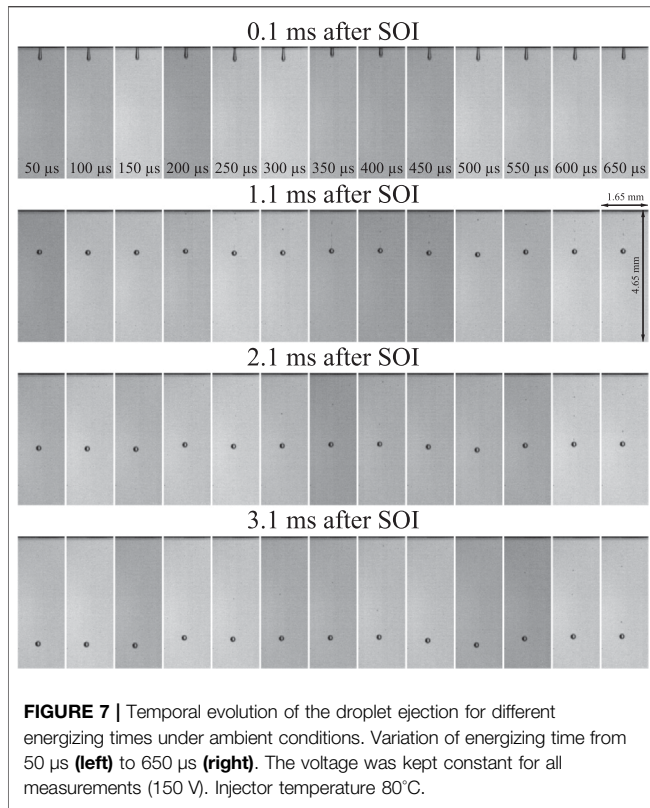
screwed front to be able to capture the motion of the needle. An example sequence for largest needle lift (250 V driving voltage) is shown in **Figure 5**. The image acquiring frequency was set at 20 kHz to capture the fast needle movement (higher sampling rates were not possible due to the low lens speed of the Navitar zoom-lens for large magnifications). Nevertheless, needle lift and return could be observed within four images (i.e. 0.15 ms).

The images have been post-processed to measure the needle lift. The setup results in a resolution of 3.5 μ m per pixel. In **Figure 6** (top) the needle lift depending on time after start of injection (SOI) and varying voltage is shown for an energizing time of 500 μ s. The needle lift shows a quite linear dependence on the driving voltage, the rising/falling edges of the lift curves have an almost identical gradient since the voltage change rate has been fixed at 3.0 V/ μ s for rising and falling voltages. The hold-phase starts later for higher voltages due to the longer delay to full lift, but the duration is exactly 500 μ s as pre-set in the injector amplifier. In all measurements, a slight overshoot of the needle lift occurs after the end of the opening phase due to piston mass and spring interaction.

In addition to the voltage, the ET was also varied at a constant driving voltage of 150 V (**Figure 6**, bottom). The results are as

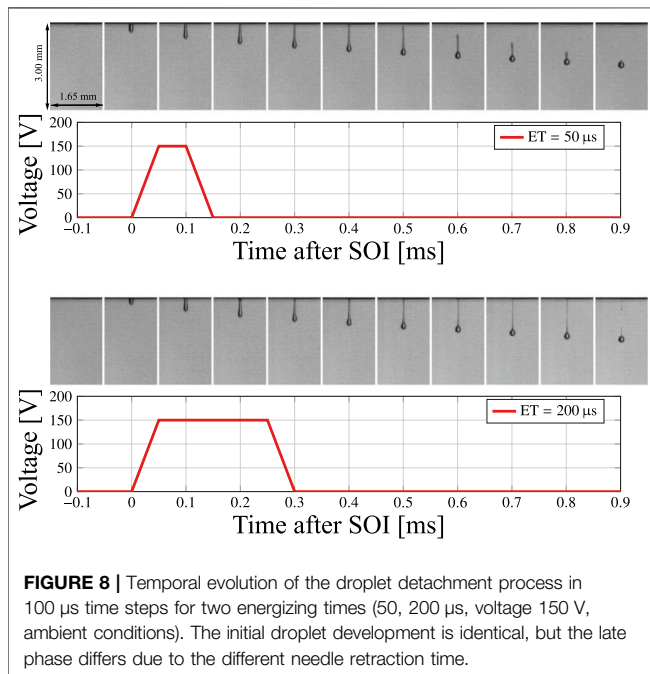
expected, with hold-phase durations corresponding to the predefined value. The measured lift fluctuates within the range of one pixel. For a hold time of 250 μ s it appears as if the needle lift starts before SOI. The reason for this behavior is the difference between trigger signal and camera internal image clock. The camera starts capturing before the trigger is set. When the manual trigger for SOI is released, the pre-captured images are shifted, whereby a maximum possible error of ± 0.5 picture must be accepted. Increasing the sample frequency would reduce this uncertainty, but this was not possible because it would have reduced the already unsatisfactory exposure time even further.





Droplet Behavior for Different Energizing Times

To investigate the influence of different energizing times on the droplets, the driving voltage was fixed to 150 V and the energizing time was varied between 50 and 650 μs with steps of 50 μs . The resulting high-speed image sequences are shown in Figure 7. As can be

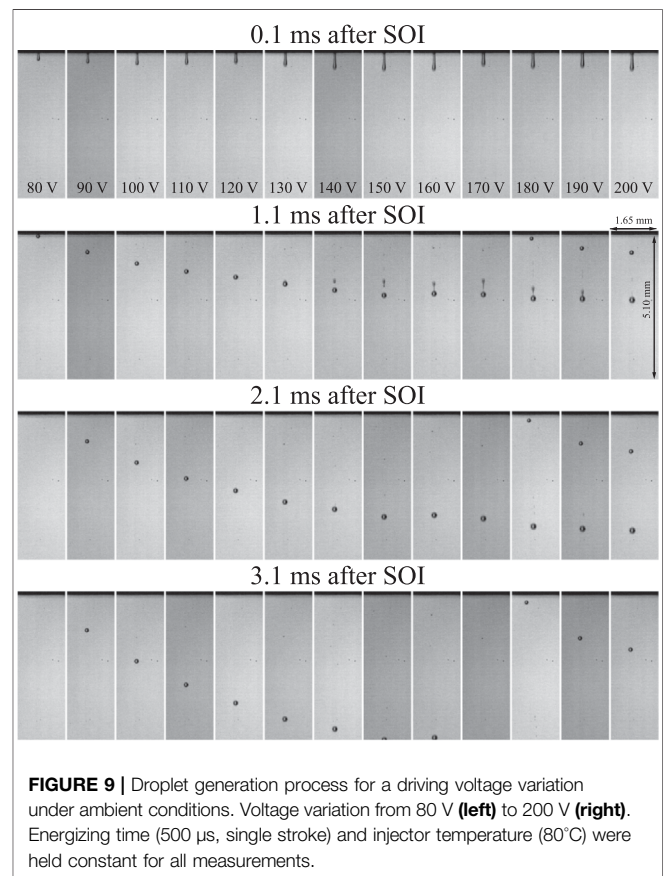


seen, the ET variation has no influence on the position (i.e. velocity) of the injected droplets. However, looking at the droplet sizes, a slight variation is observable: The diameters for 50, 100 and 150 μs ET are 5% larger than for the longer energizing times.

In Figure 8, the high-speed captures for two different energizing times are shown with the corresponding voltage profiles. The gradient of the rising edge (3.0 V/ μs) results in a voltage rise and fall time of 50 μs . Due to the trigger delay of the high-speed camera, the tip of the ejected oil ligament is already visible in the first image. Removing the voltage earlier for shorter ET's "cuts off" the oil ligament at the nozzle exit when the needle returns, therefore the whole ejected oil volume merges into the droplet. For longer ET's, the ligament between nozzle and droplet has more time to form itself (is not affected by the return of the needle) and separates somewhere in the middle between nozzle exit and droplet. Therefore a part of the ejected oil volume is pulled back into the nozzle, resulting in slightly smaller droplet sizes for energizing times higher than 200 μs .

Droplet Generation Behavior for Different Driving Voltages

Since the driving voltage is the main parameter to control the displacement of the piezo stack and therefore the needle lift, the droplet generation process depending on the needle lift has been investigated more closely. To ensure comparable conditions across all experiments, the PZDI and thus the oil reservoir in the nozzle plate was heated to 80°C (at ambient temperatures 21°C no droplet



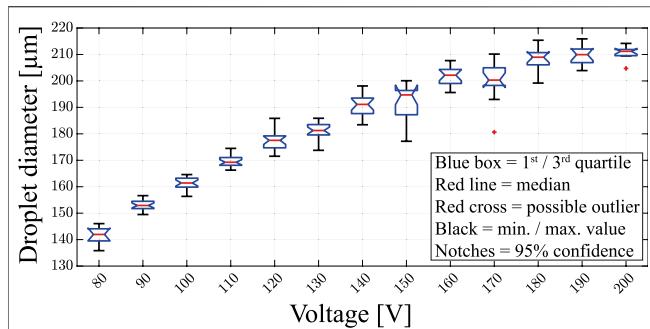


FIGURE 10 | Boxplots of the measured droplet diameters (analyzed between 2 and 4 ms after SOI) in function of the driving voltage for a constant energizing time of 500 μ s under ambient conditions. A significant difference between the median diameters can be observed for lower voltages.

detachment could be observed). Starting with 80 V and a constant energizing time of 500 μ s (Figure 9, left), the voltage was increased in steps of 10 V up to 200 V (Figure 9, right). The top row of images shows how a ligament is pushed out 0.1 ms after SOI. It can be observed that higher voltages push out longer ligaments. The lowest driving voltage of 80 V leads to detachment of a single oil droplet, which is, however, pulled back due to surface tension before it can detach itself. All voltages below 80 V showed this behavior. For voltages in the range of 140–200 V, the volume displaced by the needle is large enough to cause the formation of multiple droplets. Voltages between 140 and 170 V generate smaller satellite droplets, but since they are still connected to the first droplet with ligaments even after separation from the nozzle, the surface tension pulls them forward into the first droplet. This phenomenon is also noticeable for 180–200 V, but here the ejected oil volume was large enough to generate a second, independent droplet with a lower velocity, it does no longer merge with the first one. A special case can be seen for 180 V: The velocity of the second droplet is nearly zero. This occurs because the surface tension in the ligament initially connecting it to the nozzle was able to slow down the emerging droplet to almost a stop before it was detached.

The detected droplet diameters for each image frame between 2.0 and 4.0 ms (i.e. after the droplets are fully developed) are shown as notched boxplots in Figure 10. It shows that the droplet diameter does depend on the driving voltage — higher voltages generate larger droplets (range from 140 to 210 μ m). The measured size variation after full development of the droplets is mostly due to inaccuracies in the detection of the droplet contour. The notches of the blue boxes represent the 95% confidence interval for the median. So, if the notches of two different boxes do not overlap, it can be concluded that the true median (with 95% confidence) are indeed different. As can be seen, for lower voltages up to 130 V the generated droplet sizes are clearly different. For higher voltages however, at least one of the neighboring confidence interval notches does overlap — these detected droplet sizes do not differ significantly.

By using the detected position at every time step, the droplet speed can be calculated (for the first droplet only, Figure 11). As mentioned before, a higher driving voltage results in a higher droplet speed. Since the voltage increase rate was fixed at 3.0 V/ μ s, the needle velocity and therefore the velocity of the ejected oil

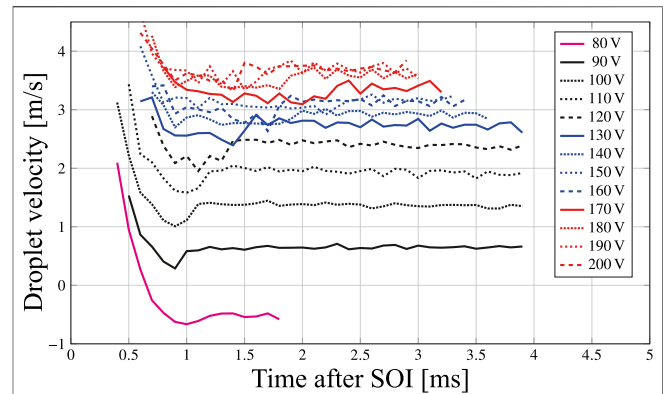


FIGURE 11 | Droplet speed calculated from the tracked droplet positions for a variation of the driving voltage (energizing time 500 μ s, ambient conditions). A special case occurs for the lowest driving voltage (80 V) — here the droplet reverses its direction and moves back to the orifice!

should be identical for all cases. What differs is the actual full needle lift, and thus the duration of the oil ejection phase. For lower voltages, the end of oil ejection happens earlier, and the ligament detachment process starts earlier as well due to the lack of following oil. This faster droplet formation can be observed in the early detection of the droplets in Figure 11 (voltages up to 100 V, before 0.5 ms). Another effect can be observed for voltages up to 120 V. The droplets are slowed down considerably in the first few 100 microseconds. The speed of the droplet is decreased by surface tension forces during the stretching and constriction of the initially existing oil ligament between droplet and nozzle. The actual detachment of the droplet from the nozzle takes place somewhere before the minimal droplet velocity (i.e. detachment from nozzle around 0.75 ms for 100 V). After minimal velocity, the detached ligament merges with the droplet due to surface tension and accelerates it due to the momentum addition. For higher driving voltages, this behavior of the initially decreasing velocity is also recognizable. But since the generated droplet diameter and thus its mass is considerably larger, the effect is not as strong, the resulting final velocity is higher for larger droplets. A special case can be seen for 80 V. The droplet velocity is decreased so much by the aforementioned mechanism that the direction reverses, the droplet moves back to the nozzle plate and disappears after 1.75 ms.

The reproducibility in terms of droplet diameter with the same driving voltage (150 V) was investigated with 21 injections. Therefore, the recognized droplet diameter for every image of the fully developed droplets (31 pictures for every shot) was used to calculate the mean value as well as the standard deviation. This corresponds to an uncertainty of the recognition algorithm of approximately 5 μ m. Since one pixel corresponds to approx. 3.5 μ m, this is the main source of error.

Experiments in the Constant Volume Combustion Chamber CVCC Under Elevated Pressures and Temperature

The PZDI was mounted in the CVCC and the optical setup was adapted (see Figure 4). The PZDI was installed in its adapter that

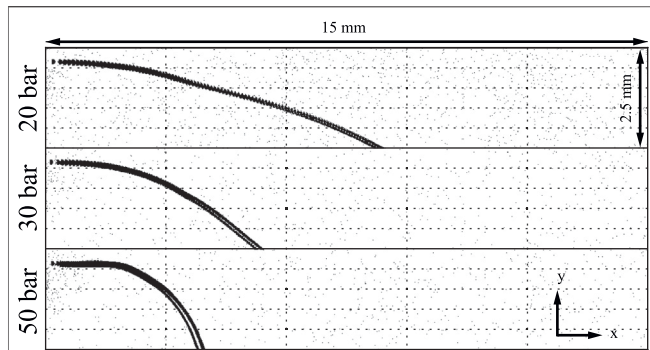


FIGURE 12 | Superimposed set of captures (500 images) of the droplet path in the CVCC under elevated pressures. The penetration length in x -direction (horizontal) is decreasing with increasing gas density, gravity pulls the droplets downwards. Image frequency 5 kHz, energizing time 500 μ s, driving voltage 150 V, CVCC and injector temperature 80°C, CVCC filled with nitrogen.

allows for thermal conditioning. Due to safety reasons the cell was always filled with nitrogen instead of air. For more information about the cell cf. (Schneider, 2003). To avoid the turbulence generated by the cell gas intake process, droplet injection started 1.5 s after cell inlet valve closing. Thanks to the pressure equalization bores in the nozzle plate (see **Figure 2**) the large pressure gradient during the cell filling process did not impair the droplet generation process.

In **Figure 12**, a set of superimposed captures (500 images) visualize the droplet movement respectively droplet path for a variation of cell pressure (constant energizing time 500 μ s, driving voltage 150 V). Higher gas pressures lead to higher drag of the droplets and cause a shorter penetration length in horizontal direction. The white line that can be observed in the middle of the droplet path toward the end of the path (especially for 50 bar cell pressure) is an artifact of the illumination technique used for these experiments: The xenon light source at the bottom was switched off, therefore only the “front” and “back” end of the droplets reflect light into the camera.

As shown for ambient conditions (**Figure 9**), higher driving voltages cause the ejection of multiple droplets, whereby the first one has a higher momentum and consequently larger penetration length (for driving voltages of 200 and 250 V, cell pressure 60 bar, **Figure 13**). The droplet velocity in horizontal direction (x -axis) slows down due to the drag, at the same time the vertical droplet velocity (y -axis) rises due to the gravity. A higher velocity results in a longer separation between the individual droplet images. Toward the end, when velocity is very low, the droplet images overlap. Especially at the lowest driving voltage it can be seen that the droplet trajectory is also affected by the residual flow/turbulence in the cell—the droplet moves slightly upwards after injection.

The horizontal droplet penetration diagrams shown in **Figure 14** are based on the tracking of the position of the first droplet only. At the lowest driving voltage of 150 V (where only single droplets are ejected) a maximum penetration length (x -direction) of 7.5 mm can be measured for a cell pressure of

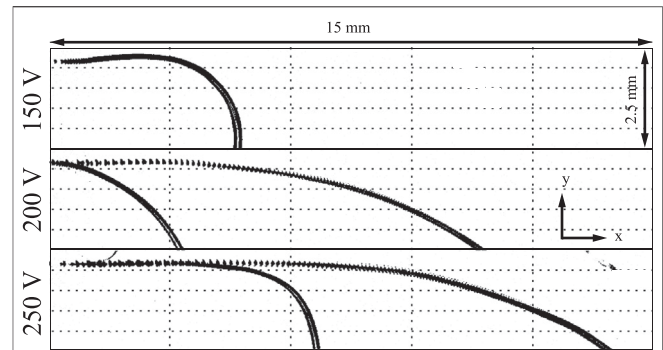


FIGURE 13 | Superimposed images of the droplet paths for three different driving voltages in the CVCC. Although only one needle stroke was made, multiple droplets were ejected at driving voltages of 200 and 250 V. Image frequency 5 kHz, energizing time 500 μ s, CVCC and injector temperature 80°C, CVCC filled with nitrogen at 60 bar.

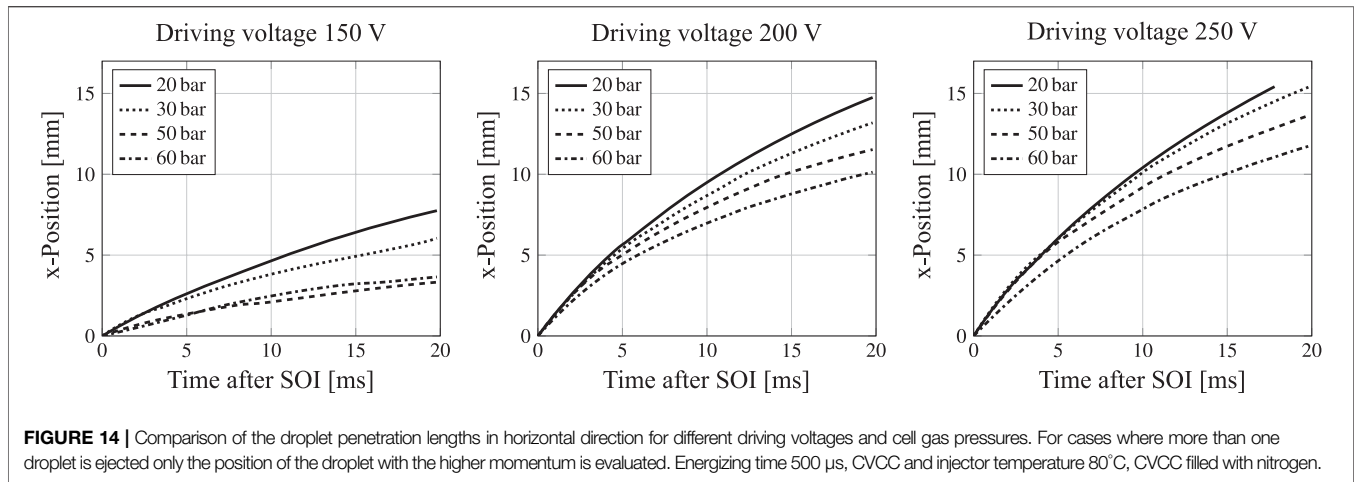
20 bar ($\rho_{\text{gas}} \approx 18 \text{ kg/m}^3$). For higher cell pressures, the penetration length of the droplets decreases to less than 5 mm. Higher driving voltages of the injector lead to larger needle lifts, thus more oil is injected with higher velocities. Consequently, the largest penetration lengths (for the first droplets only) are achieved with the highest driving voltage (250 V), where the droplet leaves the observable range of 15 mm after 20 ms. Whereas the droplet penetration plots for 200 and 250 V driving voltage show the expected influence of the cell gas density, some irregularities can be observed for a driving voltage of 150 V—the penetration length is not uniformly influenced by the cell pressure. These discrepancies are caused by the residual flow/turbulence in the cell which has more influence on the smaller and more slow droplets generated with lower driving voltages.

SUMMARY/CONCLUSION

A novel kind of injector that is able to create small, distinct lube oil droplets was designed, manufactured, and characterized. In this injector, a needle ($\varnothing_{\text{needle}} = 290 \mu\text{m}$) is moving in a slightly larger bore which is filled with lube oil. The needle pushes the oil volume in the bore, which causes the ejection of droplets through the nozzle at the end of the bore (hole diameter 100 μm). The needle is actuated with a piezo stack from a standard GDI injector where an applied voltage causes a proportional lengthening of the stack due to the piezoelectric effect (up to 65 μm).

The effect of different driving voltages (i.e. needle lifts) and energizing times (i.e. duration of the needle lift) on the droplet generation process have been investigated under both ambient and elevated pressures/temperature conditions. Experiments at higher pressures and temperature levels have been performed in a constant volume combustion chamber (CVCC) filled with nitrogen. The droplet formation process including size and movement of the thereby generated droplets have been analyzed with optical measurement techniques using high-speed cameras.

The diameter of the generated droplets was found to be in a range of 140–210 μm depending on the piezo stack voltage (i.e.



needle lift). The displaced oil volume due to the needle lift is larger than the volume of the generated droplet, it was found that a part of the ejected oil is drawn back into the bore when the needle moves back due to surface tension effects. Larger needle lifts (i.e. higher driving voltages of the piezo stack) can cause the ejection of a second, trailing droplet which has, however, less momentum than the first one.

It could be shown that the droplet generation process is not impaired by higher pressure levels (up to 60 bar) and the high pressure gradients (due to the filling process) in the CVCC. As expected, increasing nitrogen densities slows down the ejected droplets, thus decreasing penetration lengths.

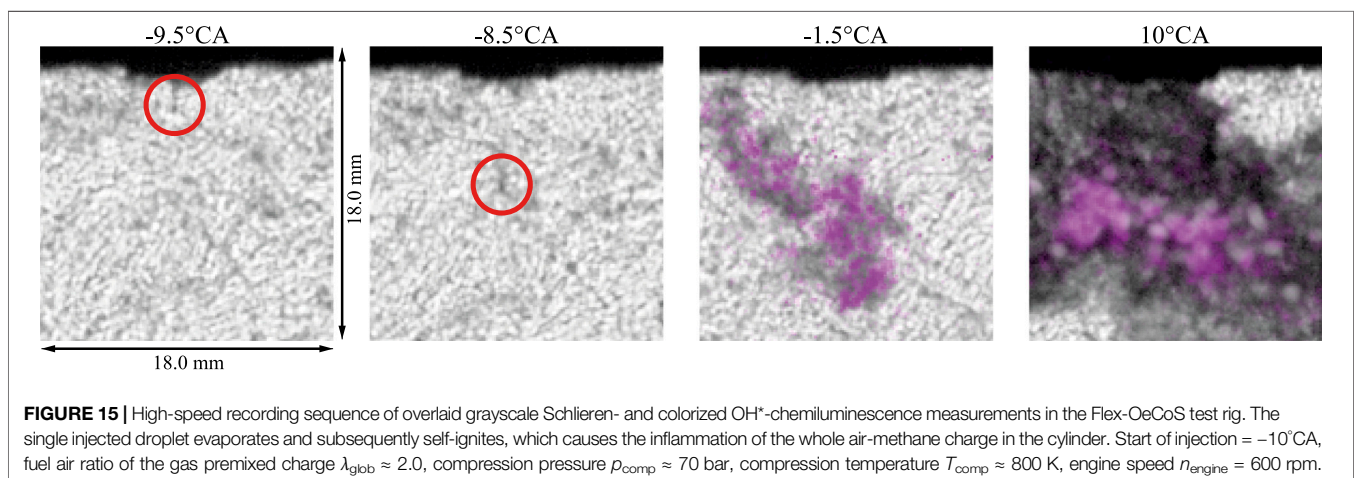
The injector exhibits a very reproducible behavior as long as the injector and lube oil reservoir temperature is kept constant. For this purpose, the injector was mounted in a specially designed adapter and connected to an external temperature control unit.

This new injector now allows to inject distinct, small lube oil droplets with known sizes into engine cylinders or combustion chambers at engine relevant conditions, thereby enabling further fundamental investigations of lube oil induced pre-ignition phenomena in dual-fuel combustion engines.

OUTLOOK

Undesired self-ignition of premixed gas-air charges in dual-fuel engines caused by burning lube oil droplets continue to endanger both performance and structural integrity of those engines. Consequently, this topic remains an important part of research in the field of combustion engines. However, since experimental investigations in large marine engines are difficult and associated with enormous costs it is important to be able to investigate these phenomena in smaller scale, but under nonetheless realistic, engine like conditions. Such investigations then allow for the development and validation of suitable CFD models, which in turn can be used in large engine simulations.

As a first step, an injector able to produce small lube oil droplets under both ambient conditions and at elevated pressure levels has been presented in this work including corresponding measurements. The next step is to use this injector for lube oil droplet injection under realistic, engine like conditions, both with and without premixed gas-air cylinder charges. An ideal experimental test facility for such investigations is the “Flex-OeCoS” (Flexibility regarding Optical engine Combustion diagnostics and/or development of corresponding Sensing



devices) test rig located at the Institute of Thermal and Fluid Engineering of the University of Applied Sciences and Arts Northwestern Switzerland. A detailed explanation of the test rig can be found in (Schneider et al., 2020). With its optically accessible cylinder head, pre-ignition phenomena during dual-fuel operation under engine-relevant conditions can be observed and investigated very well. The flexible test rig can be operated in many different combustion modes, a report about a measurement campaign in a dual-fuel configuration can be found in (Humair et al., 2020).

The next experimental investigations are focused on the droplet ignition behavior, and whether the ignited oil droplets can cause ignition of the whole pre-mixed charge. A first measurement of an injected lube oil droplet into the hot, compressed methane-air charge in the combustion chamber of the Flex-OeCoS is shown in **Figure 15**. The grayscale image is the image from the Schlieren setup, it is overlaid with the simultaneously acquired, magenta colored image of OH^{*}-chemiluminescence. The droplet was injected at -10°CA (before TDC) and is marked with a red circle in the images taken at -9.5°CA and -8.5°CA respectively. Later, an ignition can be seen in the magenta colored OH^{*}-chemiluminescence image in the region where the evaporated lube oil is expected to be (-1.5°CA). The ignition of the lube oil vapor results in flame kernels which subsequently ignite the whole gas-air charge in the combustion chamber (10°CA).

REFERENCES

- Atherton, T. J., and Kerbyson, D. J. (1999). Size invariant circle detection. *Image Vis. Comput.* 17, 795–803. doi:10.1016/S0262-8856(98)00160-7
- Christensen, O. (2010). Cylinder lubrication of two-stroke crosshead marine diesel engines. *Wärtsilä Tech. J.*, 39–48.
- Dahnz, C., Han, K.-M., and Magar, M. (2009). *Vorentflammung bei Ottomotoren*. Germany: Research Association on Combustion Engines e.V (FVV), 931.
- Humair, D., Cartier, P., Süess, P., Wüthrich, S., Herrmann, K., Barro, C., et al. (2020). “Characterization of dual-fuel combustion processes,” in Sixth large engine symposium rostock/6. Rostocker Großmotorentagung 2020, Rostock, DE, September 3–4, 2020.
- Imhof, D., and Takasaki, K. (2012). Visual combustion research using the rapid compression expansion machine. *MTZ Ind.* 2, 28–39. doi:10.1365/s40353-012-0037-6
- Imhof, D. (2013). Visual combustion studies for environmental friendly marine diesel and gas engines. PhD thesis. Fukuoka, (JP): Kyushu University Japan.
- Kaewtrakulpong, P., and Bowden, R. (2002). An improved adaptive background mixture model for real-time tracking with shadow detection. *Video-Based Surveillance Systems*, 135–144. doi:10.1007/978-1-4615-0913-4_11
- Long, Y., Wang, Z., Qi, Y., Xiang, S., Zeng, G., Zhang, P., et al. (2016). Technical Paper. Effect of oil and gasoline properties on pre-ignition and super-knock in a thermal research engine (TRE) and an optical rapid compression machine (RCM), SAE International. doi:10.4271/2016-01-0720
- Mayer, M., Hofmann, P., Williams, J., and Tong, D. (2016). Influence of the engine oil on pre-ignitions at highly supercharged direct-injection gasoline engines. *MTZ Worldw.* 77, 36–41. doi:10.1007/s38313-016-0044-z
- Ohtomo, M., Miyagawa, H., Koike, M., Yokoo, N., and Nakata, K. (2014). Pre-ignition of gasoline-air mixture triggered by a lubricant oil droplet. *SAE Int. J. Fuels Lubr.* 7 (3), 673–682. doi:10.4271/2014-01-2627

DATA AVAILABILITY STATEMENT

The raw data supporting the conclusion of this article will be made available by the authors, without undue reservation.

AUTHOR CONTRIBUTIONS

All authors have read and agree to the published version of the manuscript. Conceptualization, PS, BS, KH; Investigation, PS; DW; Supervision, KH; Writing, PS, BS, KH; Review, PS, BS, KH, DW, SW.

FUNDING

Financial support of the Swiss Federal Office of Energy (SFOE) is gratefully acknowledged.

ACKNOWLEDGMENTS

We thank R. Bombach (Paul Scherrer Institute) for the support in terms of optical equipment and measurements at the CVCC.

- Palaveev, S. (2013). *Vorentflammung bei Ottomotoren II*. Germany: Research Association on Combustion Engines e.V. (FVV), 1051.
- Schneider, B. (2003). Experimentelle Untersuchungen zur Spraystruktur in transienten, verdampfenden und nicht verdampfenden Brennstoffstrahlen unter Hochdruck. PhD thesis. Zürich, (CH): ETH Zürich. doi:10.3929/ethz-a-004522641
- Schneider, B., Schürch, C., Boulouchos, K., Herzig, S., Hangartner, M., Humair, D., et al. (2020). The Flex-OeCoS- a novel optically accessible test rig for the investigation of advanced combustion processes under engine-like conditions. *Energies* 13 (7), 1794. doi:10.3390/en13071794
- Welling, O., Moss, J., Williams, J., and Collings, N. (2014). Measuring the impact of engine oils and fuels on low-speed pre-ignition in downsized engines. *SAE Int. J. Fuels Lubr.* 7 (1), 1–8. doi:10.4271/2014-01-1219
- Yasueda, S., Takasaki, K., and Tajima, H. (2012). “The abnormal combustion affected by lubricating oil ignition in premixed gas engines,” in Proceedings of the ASME 2012 internal combustion engine division spring technical conference, Torino, Piemonte, Italy, May 6–9, 2012, 6–9. doi:10.1115/ICES2012-81042
- Yasueda, S., Takasaki, K., and Tajima, H. (2013). Abnormal combustion caused by lubricating oil in high BMEP gas engines. *MTZ Ind.* 3, 34–39. doi:10.1007/s40353-013-0069-6

Conflict of Interest: The authors declare that the research was conducted in the absence of any commercial or financial relationships that could be construed as a potential conflict of interest.

Copyright © 2021 Süess, Schneider, Wüthrich, Wüthrich and Herrmann. This is an open-access article distributed under the terms of the Creative Commons Attribution License (CC BY). The use, distribution or reproduction in other forums is permitted, provided the original author(s) and the copyright owner(s) are credited and that the original publication in this journal is cited, in accordance with accepted academic practice. No use, distribution or reproduction is permitted which does not comply with these terms.